

# Facial Action Unit Detection Using Attention and Relation Learning

Zhiwen Shao<sup>1</sup>, Zhilei Liu<sup>2</sup>, Jianfei Cai<sup>3</sup>, Yunsheng Wu<sup>4</sup>, Lizhuang Ma<sup>5,1</sup>

<sup>1</sup> Department of Computer Science and Engineering, Shanghai Jiao Tong University, China

<sup>2</sup> School of Computer Science and Technology, Tianjin University, China

<sup>3</sup> School of Computer Science and Engineering, Nanyang Technological University, Singapore

<sup>4</sup> Tencent YouTu, China

<sup>5</sup> School of Computer Science and Software Engineering, East China Normal University, China

shaozhiwen@sjtu.edu.cn, zhileiliu@tju.edu.cn, asjfcai@ntu.edu.sg

simonwu@tencent.com, ma-lz@cs.sjtu.edu.cn

## Abstract

Attention mechanism has recently attracted increasing attentions in the area of facial action unit (AU) detection. By finding the region of interest (ROI) of each AU with the attention mechanism, AU related local features can be captured. Most existing attention based AU detection works use prior knowledge to generate fixed attentions or refine the predefined attentions within a small range, which limits their capacity to model various AUs. In this paper, we propose a novel end-to-end weakly-supervised attention and relation learning framework for AU detection with only AU labels, which has not been explored before. In particular, multi-scale features shared by each AU are learned firstly, and then both channel-wise attentions and spatial attentions are learned to select and extract AU related local features. Moreover, pixel-level relations for AUs are further captured to refine spatial attentions so as to extract more relevant local features. Extensive experiments on BP4D and DISFA benchmarks demonstrate that our framework (i) outperforms the state-of-the-art methods for AU detection, and (ii) can find the ROI of each AU and capture the relations among AUs adaptively.

## Introduction

Facial action unit (AU) detection is an important face analysis task. It recognizes facial expressions by analyzing cues of some atomic muscle movements in local facial regions. A very comprehensive set of facial atomic muscle movements, namely AUs, is defined by Facial Action Coding System (FACS) (Ekman and Rosenberg 1997). On the other hand, attention mechanism has been adopted in various structural prediction tasks such as saliency detection (Kuen, Wang, and Wang 2016), object recognition (Xiao et al. 2015), and image captioning (You et al. 2016), where great success has been achieved. It is natural to apply the attention mechanism to find the region of interest (ROI) of each AU so that more relevant local features can be captured. However, in literature there are only a few attention based AU detection methods being proposed, in which prior knowledge is required to predefine the attentions of AUs.

Since facial landmarks can provide rough locations of AUs, they have been used for defining the AU attentions. Li et al. (Li et al. 2017; Li, Abtahi, and Zhu 2017) proposed a deep learning based method using predefined attentions for AU detection, in which landmarks are used to generate the ROI with a fixed size and a fixed attention distribution

for each AU. Sanchez et al. (Sanchez, Tzimiropoulos, and Valstar 2018) utilized an hourglass network (Newell, Yang, and Deng 2016) for AU intensity estimation by regressing from the input image to attention maps, where the ground-truth attention maps are defined by landmarks and AU intensities with a Gaussian distribution. These methods design fixed attentions based on the prior knowledge about the location relationship between AUs and landmarks, which are handcrafted and have limited capacity to model various non-rigid AUs. Shao et al. (Shao et al. 2018) proposed a deep learning based joint AU detection and face alignment framework with an adaptive attention learning module, which is a pioneering work of adaptive attention learning for AU detection. However, the refined attentions are very similar to initial attentions predefined by landmarks, in the sense that each refined attention only smooths out the shape and attention distribution of predefined ROI and the locations beyond the ROI still have uniform attention weights.

In addition, the relations among AUs should be utilized to capture more accurate attentions. Although the AU-level relations have been exploited for AU detection in literature, they have not been integrated with the attention mechanism. Therefore, in this paper we propose a novel deep learning based weakly-supervised attention and relation learning (WSARL) framework for AU detection. Only AU labels are used to learn the implicit attentions and relations adaptively, without being restricted by the predefined attentions like Shao et al. (Shao et al. 2018). In particular, multi-scale features shared by each AU are learned firstly, and then both channel-wise attention learning and spatial attention learning are used to select and extract AU related local features. Moreover, we propose a pixel-level relation learning method to refine spatial pixel-wise attentions of each AU so as to extract more relevant local features. The entire framework is end-to-end for joint learning of attention and relation, without any post-processing step.

The contributions of this paper are threefold. First, a weakly-supervised attention learning method is proposed for AU detection, where both channel-wise attentions and spatial attentions are learned with only AU labels. Second, pixel-level relation learning for each AU is proposed to capture the relations among AUs, where spatial attentions are refined to extract more relevant local features. Third, extensive experiments demonstrate that our framework WSARL

outperforms the state-of-the-art AU detection methods, and can find the ROI of each AU and capture the relations among AUs adaptively.

## Related Work

In this section, we review both attention based facial AU detection methods and relation based facial AU detection methods, since our framework is mainly composed of channel-wise and spatial attention learning and pixel-level relation learning.

### Attention Based Facial AU Detection

It is hard to define the attentions of each AU manually, since AUs have no distinct contour and texture and may change across persons and facial expressions. A few recent methods use facial landmarks to define the attentions of each AU based on prior knowledge. Li et al. (Li et al. 2017; Li, Abtahi, and Zhu 2017) proposed an Enhancing and Cropping Net (EAC) for AU detection by using predefined attentions to enhance and crop the ROIs of AUs. The ROI of each AU has a fixed size and a fixed attention distribution, whose location is given by landmarks. Sanchez et al. (Sanchez, Tzimiropoulos, and Valstar 2018) employed an hourglass network (Newell, Yang, and Deng 2016) for attention map regression to estimate all AU intensities. Similarly, the ground-truth attention map of each AU is predefined with a Gaussian distribution, where landmarks determine the center and AU intensities determine the amplitude and size. Shao et al. (Shao et al. 2018) proposed a deep learning based joint AU detection and face alignment framework called JAA, which uses an adaptive attention learning module to adaptively refine initial attentions of each AU predefined by landmarks. The shape and the attention distribution of the predefined ROI are only smoothed and correlated regions beyond the predefined ROI are not highlighted.

All these methods demonstrate the effectiveness of attention mechanism for AU detection. However, they all use fixed attentions or refine the attentions within a small range, which limits their capacity to model various AUs.

### Relation Based Facial AU Detection

AU detection is a multi-label classification problem, where the relations among AUs can be exploited to improve the performance. Zhang et al. (Zhang and Mahoor 2016) proposed a multi-task multiple kernel learning method to learn a kernel representation which encodes the AU relations. Zhao et al. (Zhao et al. 2016) proposed a Joint Patch and Multi-Label Learning (JPML) framework for AU detection by modeling the joint dependence behind features, AUs, and their interplay. Two AU relations, positive correlation and negative competition, are computed by statistically analyzing the training datasets. Wu et al. (Wu and Ji 2016) utilized a cascade regression framework to capture global AU relations and global dependencies between AUs and landmarks. Eleftheriadis et al. (Eleftheriadis, Rudovic, and Pantic 2015) proposed a multi-conditional latent variable model to jointly detect multiple AUs based on handcrafted features, in which both local and global dependencies among AUs are encoded.

These methods exploit AU-level relations without integrating with the attention mechanism. In contrast, we employ an end-to-end deep learning framework to model the pixel-level relations for each AU. Our proposed pixel-level relation learning is integrated with the attention learning to capture both attentions and relations of AUs.

## WSARL for Facial AU Detection

### Overview

Our proposed framework WSARL is shown in Figure 1, including three modules, multi-scale region learning, attention learning, and relation learning. In particular, the multi-scale region learning extracts features of multi-scale local regions as the foundation of our framework. The learned multi-scale features are then shared by each AU to facilitate the attention learning and relation learning. Moreover, the integration of attention learning and relation learning is the central part for AU detection, which learns channel-wise attentions, spatial attentions, and pixel-level relations adaptively for each AU with an independent branch respectively.

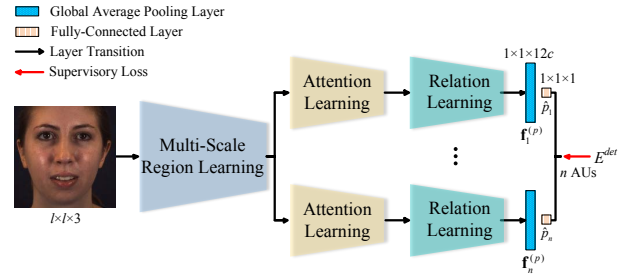


Figure 1: Architecture of the proposed WSARL framework, where each AU has the same structure of attention learning and relation learning.

As illustrated in Figure 1, the input to our framework is a color face image with a size of  $l \times l \times 3$ . After the attention and relation learning, for the  $i$ -th AU,  $i = 1, \dots, n$ , the finally learned AU related feature denoted as  $\mathbf{f}_i^{(p)} \in \mathbb{R}^{12c \times 1}$  is obtained using the Global Average Pooling layer (Lin, Chen, and Yan 2014), where  $n$  is the number of AUs, and  $c$  is a hyperparameter with respect to the structure of our framework. Then the estimated AU occurrence probability is computed with a sigmoid function  $\sigma(\cdot)$  as

$$\hat{p}_i = \sigma(\mathbf{w}_i^{(p)T} \mathbf{f}_i^{(p)}), \quad i = 1, \dots, n, \quad (1)$$

where  $\mathbf{w}_i^{(p)} \in \mathbb{R}^{12c \times 1}$  denotes the weight parameters of the last one-dimensional fully-connected layer. Without loss of generality, we simplify the notation of the linear mapping  $\mathbf{w}_i^{(p)T} \mathbf{f}_i^{(p)}$  by omitting the bias term.

Most of the AU detection benchmarks suffer from the imbalance of occurrence rates of AUs (Martinez et al. 2017), which is harmful to training. Similar to JAA (Shao et al. 2018), we weight the loss of each AU to alleviate the data imbalance issue. In particular, we use the weighted sigmoid

cross entropy loss for AU detection formulated as

$$E^{det} = \sum_{i=1}^n w_i [p_i \log \hat{p}_i + (1 - p_i) \log(1 - \hat{p}_i)], \quad (2)$$

where  $p_i$  and  $w_i$  denote the ground-truth occurrence probability and the weight of the  $i$ -th AU, respectively.  $w_i$  is inversely proportional to the occurrence rate of the  $i$ -th AU in the training set.

### Multi-Scale Region Learning

Considering that different AUs occur in different multi-scale regions, Shao et al. (Shao et al. 2018) proposed a hierarchical and multi-scale region layer to process multi-scale local patches with independent convolutional filters, where the intermediate convolutional layers with different numbers of partitioned patches are stacked. Considering the overall neural network already consists of stacked layers, we simplify the hierarchical and multi-scale region layer by removing the hierarchical structure.

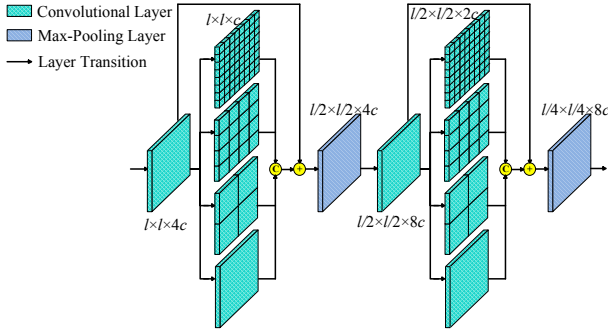


Figure 2: Architecture of the multi-scale region learning module, where  $l \times l \times c$  indicates that the height, width, and channel of the corresponding layer are  $l$ ,  $l$ , and  $c$  respectively, and “C” and “+” denote concatenation and element-wise sum respectively.

Figure 2 shows the architecture of the multi-scale region learning module. It consists of two blocks of multi-scale region layer, each of which is followed by a max-pooling layer over  $2 \times 2$  spatial fields with a stride 2. A block of multi-scale region layer contains an input convolutional layer and four intermediate convolutional layers, each of which uses  $3 \times 3$  convolution filters with a stride 1 and a padding 1. The feature map of the input layer is followed by Batch Normalization (BN) (Ioffe and Szegedy 2015) and Rectified Linear Unit (ReLU) (Nair and Hinton 2010) and is partitioned into  $8 \times 8$ ,  $4 \times 4$ ,  $2 \times 2$ , and  $1 \times 1$  patches respectively, which are fed into the four intermediate layers respectively. The feature maps of the four intermediate layers are then concatenated to integrate the extracted multi-scale local features, and further summed element-wisely with the feature map of the input layer, finally followed by BN and ReLU. Our proposed module of the multi-scale region learning extracts rich local features which contribute to the subsequent attention learning and relation learning of each AU.

### Attention Learning

The structure of the attention learning and relation learning of a certain AU is illustrated in Figure 3. In this section, we elaborate our proposed attention learning method.

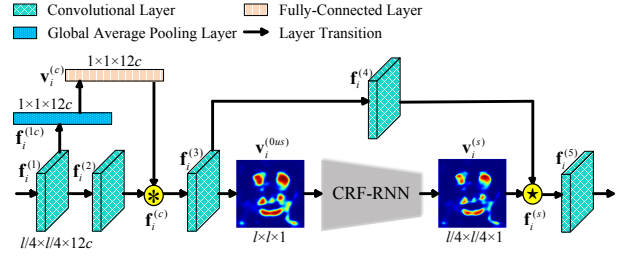


Figure 3: Architecture of the attention learning and relation learning of an example AU 7, where all the convolutional layers have the same size of  $l/4 \times l/4 \times 12c$ , and “\*” and “\*” denote channel-wise multiplication and element-wise multiplication, respectively.

As shown in Figure 3, for the  $i$ -th AU, we apply a convolution operation on the output of the multi-scale region learning module and obtain a feature  $\mathbf{f}_i^{(1)}$ . A channel-wise feature  $\mathbf{f}_i^{(1c)} \in \mathbb{R}^{12c \times 1}$  and a feature  $\mathbf{f}_i^{(2)}$  are generated by performing Global Average Pooling and convolution on  $\mathbf{f}_i^{(1)}$ , respectively. The channel-wise attention weights  $\mathbf{v}_i^{(c)} \in \mathbb{R}^{12c \times 1}$  are computed as

$$\mathbf{v}_i^{(c)} = \sigma(\mathbf{W}_i^{(1c)T} \mathbf{f}_i^{(1c)}), \quad i = 1, \dots, n, \quad (3)$$

where  $\mathbf{W}_i^{(1c)} \in \mathbb{R}^{12c \times 12c}$  denotes the weight parameters of the  $12c$ -dimensional fully-connected layer, and  $\sigma(\cdot)$  is applied on each element of the vector. Then, we obtain the channel-wise weighted feature defined as

$$\mathbf{f}_i^{(c)} = \mathbf{v}_i^{(c)} * \mathbf{f}_i^{(2)}, \quad i = 1, \dots, n, \quad (4)$$

where  $*$  denotes the channel-wise multiplication of the feature map channels and the corresponding channel-wise attention weights. Considering each convolutional filter is analogous to performing a pattern detector (Zhang, Wu, and Zhu 2018) and a channel of a feature map is the response of a certain filter, our proposed channel-wise attention learning is essentially selecting related attributes.

During the process of the spatial attention learning, a feature  $\mathbf{f}_i^{(3)}$  is first generated by applying convolution on  $\mathbf{f}_i^{(c)}$ . Then, a spatial feature  $\mathbf{f}_i^{(3s)}$  with the size of  $l/4 \times l/4 \times 1$  is further learned from  $\mathbf{f}_i^{(3)}$  using a convolutional layer with one channel. To be consistent with the input face image,  $\mathbf{f}_i^{(3s)}$  is further upsampled to be  $\mathbf{f}_i^{(3us)}$  with the size of  $l \times l \times 1$  using bilinear interpolation (Chen et al. 2017). After that, the initial spatial attention weights are obtained as

$$\mathbf{v}_i^{(0us)} = \sigma(\mathbf{f}_i^{(3us)}), \quad i = 1, \dots, n, \quad (5)$$

where  $\mathbf{v}_i^{(0us)} = (v_{i1}^{(0us)}, \dots, v_{im}^{(0us)})$ , and  $m = l \times l$  is the number of pixels in the input image.

## Relation Learning

We use CRF-RNN (Zheng et al. 2015) to refine the initial spatial attentions, where the learned attentions are treated as the pixel-level relation model for each AU. Learning spatial attentions is a pixel-wise binary classification problem. Denote  $y_{ij} \in \{0, 1\}$  as the attention label of the  $j$ -th pixel for the  $i$ -th AU, where  $j = 1, \dots, m$ . In the fully-connected CRF-RNN model, the energy of a label assignment  $\mathbf{y}_i = (y_{i1}, \dots, y_{im})$  is defined as

$$E_i^{crf}(\mathbf{y}_i) = \sum_j \psi_i^u(y_{ij}) + \sum_{j < k} \psi_i^p(y_{ij}, y_{ik}), \quad (6)$$

where  $\psi_i^u(y_{ij}) = -\log P^{(0)}(y_{ij})$  is the unary potential which measures the cost of assigning label  $y_{ij}$  to the  $j$ -th pixel,  $P^{(0)}(y_{ij})$  is the initial label assignment probability of the  $j$ -th pixel, and  $\psi_i^p(y_{ij}, y_{ik})$  is the pairwise potential. Note that  $P^{(0)}(y_{ij} = 1) = v_{ij}^{(ous)}$  and  $P^{(0)}(y_{ij} = 0) = 1 - v_{ij}^{(ous)}$ . The pairwise potential is modeled with weighted Gaussian kernels as

$$\psi_i^p(y_{ij}, y_{ik}) = \mu_i(y_{ij}, y_{ik}) \left[ w_i^{(1)} \exp\left(-\frac{\|\mathbf{p}_j - \mathbf{p}_k\|^2}{2\alpha_i^2}\right) - \frac{\|\mathbf{I}_j - \mathbf{I}_k\|^2}{2\beta_i^2} + w_i^{(2)} \exp\left(-\frac{\|\mathbf{p}_j - \mathbf{p}_k\|^2}{2\gamma_i^2}\right) \right], \quad (7)$$

where  $\mu_i(\cdot, \cdot)$  is the label compatibility function,  $\mathbf{p}_j$  and  $\mathbf{I}_j$  denote the position vector and RGB color vector of the  $j$ -th pixel of the input face image, the hyperparameters  $w_i^{(1)}$  and  $w_i^{(2)}$  control the relative importance of two Gaussian kernels, and the hyperparameters  $\alpha_i$ ,  $\beta_i$ , and  $\gamma_i$  control the scale of Gaussian kernels. The first kernel in Eq. 7 enforces nearby pixels with similar color to have the same label, and the second kernel is used to enforce smoothness. We use the mean-field approximation method proposed by (Zheng et al. 2015) to learn the refined label assignment probability, denoted as  $P(y_{ij})$ , which is directly set as the refined spatial attention weight at each pixel:

$$v_{ij}^{(us)} = P(y_{ij} = 1). \quad (8)$$

Then, the refined spatial attention weights  $\mathbf{v}_i^{(us)} = (v_{i1}^{(us)}, \dots, v_{im}^{(us)})$  is further downsampled to obtain  $\mathbf{v}_i^{(s)}$  with the size of  $l/4 \times l/4 \times 1$  using bilinear interpolation. After that, the spatial weighted feature is calculated as

$$\mathbf{f}_i^{(s)} = \mathbf{v}_i^{(s)} \star \mathbf{f}_i^{(4)}, \quad i = 1, \dots, n, \quad (9)$$

where  $\star$  denotes the element-wise multiplication of each feature map channel and the spatial attention weights, and  $\mathbf{f}_i^{(4)}$  is generated by applying convolution on  $\mathbf{f}_i^{(3)}$ . As shown in Figures 1 and 3, the finally learned AU related feature  $\mathbf{f}_i^{(p)}$  is extracted by processing  $\mathbf{f}_i^{(s)}$  with a convolutional layer and a Global Average Pooling layer. Note that  $\mathbf{f}_i^{(1)}$ ,  $\mathbf{f}_i^{(c)}$ ,  $\mathbf{f}_i^{(3)}$ , and  $\mathbf{f}_i^{(s)}$  are all followed by BN and ReLU. With CRF-RNN, our proposed relation learning method exploits the relations between each pair of pixels to refine spatial pixel-wise attentions.

We combine the two losses  $E^{det}$  and  $E_i^{crf}$  from Eqs. 2 and 6, which yields the complete loss for AU detection:

$$E = E^{det} + \sum_{i=1}^n E_i^{crf}. \quad (10)$$

Our framework is end-to-end trainable, where attentions and relations are learned with the supervision from the AU detection and the mean-field approximation of CRF-RNN.

## Experiments

### Datasets and Settings

**Datasets** Our method WSARL is evaluated on two popular datasets BP4D (Zhang et al. 2014) and DISFA (Mavadati et al. 2013) for facial AU detection. Each dataset is coded with FACS (Ekman and Rosenberg 1997) by certified experts. Note that we aim at frame-level prediction, and therefore other datasets such as CK+ (Lucey et al. 2010) are not used because they only have video-level annotations.

- **BP4D** contains 23 female and 18 male participants associating with 8 sessions, i.e. 328 videos in total. These videos include about 140,000 frames coded with AU occurrence. Similar to the settings in previous works (Zhao, Chu, and Zhang 2016; Li et al. 2017), we perform subject exclusive 3-fold cross-validation with the same subject partition rule on 12 AUs.
- **DISFA** contains 27 participants with 12 females and 15 males, each of which was recorded by a video with 4,845 frames. Each frame was labeled with AU intensities from 0 to 5. Following the settings of (Zhao, Chu, and Zhang 2016; Li et al. 2017), the AU intensity equal or greater than 2 is considered as occurrence, otherwise considered as absence. Our network is initialized with the BP4D trained model and further retrained for 8 AUs using subject exclusive 3-fold cross-validation.

**Implementation Details** Similar to JAA (Shao et al. 2018), each face image is aligned to be  $200 \times 200 \times 3$  using similarity transformation, and is cropped into  $176 \times 176 \times 3$  and horizontally flipped, randomly. The hyperparameter  $l$  is thus 176, and  $c$  is chosen to be 8. Our framework is trained for up to 12 epochs using Caffe (Jia et al. 2014) with stochastic gradient descent (SGD), a mini-batch size of 8, a weight decay of 0.0005, and a momentum of 0.9. The learning rate starts with 0.006 and is multiplied by a factor of 0.3 at every 2 epochs. The pixel-level relation learning with CRF-RNN for each AU uses 10 mean-field iterations, and the hyperparameters  $w_i^{(1)}$ ,  $w_i^{(2)}$ ,  $\alpha_i$ ,  $\beta_i$ , and  $\gamma_i$  in Eq. 7 are obtained by cross validation on a small set of training data.

**Evaluation Metrics** We use two commonly used evaluation metrics: frame-based F1-score (F1-frame) and accuracy. F1-frame is defined as  $F1 = 2PR/(P + R)$ , where  $P$  and  $R$  denote precision and recall respectively. F1-frame is good for evaluating binary classification problems, especially when samples are imbalanced (Eleftheriadis, Rudovic, and Pantic 2015). The average results of F1-frame and accuracy over all AUs (Avg) are also reported, respectively. All

Table 1: F1-frame and accuracy for 12 AUs on BP4D. The best results are shown in bold and brackets, and the second best results are shown in bold.

AU	F1-Frame						Accuracy					
	LSVM	JPML	DRML	EAC	JAA	WSARL	LSVM	JPML	DRML	EAC	JAA	WSARL
1	23.2	32.6	36.4	39.0	<b>47.2</b>	<b>[50.4]</b>	20.7	40.7	55.7	68.9	<b>74.7</b>	<b>[76.2]</b>
2	22.8	25.6	<b>41.8</b>	35.2	<b>[44.0]</b>	35.1	17.7	42.1	54.5	<b>73.9</b>	<b>[80.8]</b>	<b>73.9</b>
4	23.1	37.4	43.0	48.6	<b>[54.9]</b>	<b>51.1</b>	22.9	46.2	58.8	<b>78.1</b>	<b>[80.4]</b>	76.7
6	27.2	42.3	55.0	<b>76.1</b>	<b>[77.5]</b>	74.4	20.3	40.0	56.6	<b>78.5</b>	<b>[78.9]</b>	76.6
7	47.1	50.5	67.0	72.9	<b>74.6</b>	<b>[77.1]</b>	44.8	50.0	61.0	69.0	<b>71.0</b>	<b>[73.4]</b>
10	77.2	72.2	66.3	<b>81.9</b>	<b>[84.0]</b>	81.6	73.4	75.2	53.6	77.6	<b>[80.2]</b>	<b>[77.8]</b>
12	63.7	74.1	65.8	<b>86.2</b>	<b>[86.9]</b>	<b>[86.9]</b>	55.3	60.5	60.8	84.6	<b>[85.4]</b>	<b>85.2</b>
14	<b>64.3</b>	<b>[65.7]</b>	54.1	58.8	61.9	57.8	46.8	53.6	57.0	<b>60.6</b>	<b>[64.8]</b>	60.5
15	18.4	38.1	33.2	37.5	<b>43.6</b>	<b>[48.9]</b>	18.3	50.1	56.2	78.1	<b>[83.1]</b>	<b>82.8</b>
17	33.0	40.0	48.0	<b>59.1</b>	<b>[60.3]</b>	58.8	36.4	42.5	50.0	<b>70.6</b>	<b>[73.5]</b>	69.3
23	19.4	30.4	31.7	35.9	<b>42.7</b>	<b>[48.7]</b>	19.2	51.9	53.9	81.0	<b>[82.3]</b>	<b>81.2</b>
24	20.7	<b>42.3</b>	30.0	35.8	41.9	<b>[54.2]</b>	11.7	53.2	53.9	82.4	<b>[85.4]</b>	<b>84.8</b>
Avg	35.3	45.9	48.3	55.9	<b>60.0</b>	<b>[60.4]</b>	32.2	50.5	56.0	75.2	<b>[78.4]</b>	<b>76.5</b>

Table 2: F1-frame and accuracy for 8 AUs on DISFA. The best results are shown in bold and brackets, and the second best results are shown in bold.

AU	F1-Frame						Accuracy					
	LSVM	APL	DRML	EAC	JAA	WSARL	LSVM	APL	DRML	EAC	JAA	WSARL
1	10.8	11.4	17.3	41.5	<b>43.7</b>	<b>[51.0]</b>	21.6	32.7	53.3	85.6	<b>[93.4]</b>	<b>[93.0]</b>
2	10.0	12.0	17.7	26.4	<b>[46.2]</b>	<b>32.3</b>	15.8	27.8	53.2	84.9	<b>[96.1]</b>	<b>92.0</b>
4	21.8	30.1	37.4	<b>[66.4]</b>	56.0	<b>61.3</b>	17.2	37.9	60.0	79.1	<b>[86.9]</b>	<b>83.8</b>
6	15.7	12.4	29.0	<b>[50.7]</b>	<b>41.4</b>	40.3	8.7	13.6	54.9	69.1	<b>[91.4]</b>	<b>90.7</b>
9	11.5	10.1	10.7	<b>[80.5]</b>	44.7	<b>47.6</b>	15.0	64.4	51.5	88.1	<b>95.8</b>	<b>[96.4]</b>
12	70.4	65.9	37.7	<b>[89.3]</b>	69.6	<b>74.5</b>	<b>93.8</b>	<b>[94.2]</b>	54.6	90.0	91.2	93.2
25	12.0	21.4	38.5	<b>88.9</b>	88.3	<b>[94.0]</b>	3.4	50.4	45.6	80.5	<b>93.4</b>	<b>[96.6]</b>
26	22.1	26.9	20.1	15.6	<b>[58.4]</b>	<b>56.8</b>	20.1	47.1	45.3	64.8	<b>[93.2]</b>	<b>89.2</b>
Avg	21.8	23.8	26.7	48.5	<b>56.0</b>	<b>[57.2]</b>	27.5	46.0	52.3	80.6	<b>[92.7]</b>	<b>91.9</b>

the quantitative results are reported in percentage with % being omitted.

### Comparison with State-of-the-Art Methods

We compare our method WSARL against state-of-the-art methods under the same 3-fold cross validation setting. These methods include both traditional methods, LSVM (Fan et al. 2008), APL (Zhong et al. 2015), and JPML (Zhao et al. 2016), and deep learning based methods, DRML (Zhao, Chu, and Zhang 2016), EAC (Li et al. 2017), and JAA (Shao et al. 2018). For fairness, we use the results of LSVM, APL, and JPML reported in (Zhao, Chu, and Zhang 2016; Li et al. 2017). Note that several methods like R-T1 (Li, Abtahi, and Zhu 2017) are not compared, since they process a sequence of images instead of a single image.

**Evaluation on BP4D** Table 1 reports the F1-frame and accuracy results of our method WSARL and state-of-the-art methods on BP4D. It can be observed that WSARL outperforms all the state-of-the-art methods on the challenging BP4D benchmark for F1-frame results. JAA (Shao et al. 2018) is the latest work with outstanding performance, which is also based on deep learning and attention mechanism. Unlike JAA which uses both AU and landmark labels, WSARL achieves competitive performance with only AU

labels, which demonstrates the effectiveness of our proposed weakly-supervised attention and relation learning.

**Evaluation on DISFA** The F1-frame and accuracy results evaluated on DISFA benchmark are shown in Table 2, where it can be seen that our WSARL significantly outperforms all the previous works with large margins. Note that there is a severer data imbalance problem (Li et al. 2017) in DISFA than BP4D, which causes significant performance fluctuations for different AUs in most of the previous methods especially LSVM and APL. In contrast, in addition to top results in average F1-frame and average accuracy, WSARL exhibits more stable performance for each AU.

### Ablation Study

In this section, we conduct experiments to evaluate the effectiveness of each component in our framework. Table 3 summarizes the structures and F1-frame results of different variants of our proposed WSARL. B-Net is a baseline network with plain convolutional layers, pooling layers, and fully-connected layers, whose corresponding parts are replaced with the proposed components for different variants of WSARL.

Table 3: F1-frame for 12 AUs of different variants of our proposed WSARL on BP4D. **S**: Spatial attention. **C**: Channel-wise attention. **H**: Hierarchical and multi-scale region layer (Shao et al. 2018). **M**: Multi-scale region layer. **P**: Pixel-level relation learning. The best results are shown in bold.

Method	S	C	H	M	P	1	2	4	6	7	10	12	14	15	17	23	24	Avg
B-Net						42.0	30.5	49.4	70.5	74.3	79.3	81.7	55.7	33.5	55.7	44.6	49.5	55.6
S-Net	✓					45.1	30.4	46.3	72.2	74.6	76.9	84.7	53.7	42.8	58.3	40.9	48.2	56.2
SC-Net	✓	✓				40.4	30.4	47.7	70.5	75.4	80.2	83.3	<b>58.5</b>	44.6	57.4	43.3	47.3	56.6
SCH-Net	✓	✓	✓			46.4	38.3	49.2	74.1	74.1	78.4	85.8	57.4	44.3	<b>59.1</b>	<b>49.0</b>	48.3	58.7
SCM-Net	✓	✓		✓		49.2	<b>38.9</b>	49.2	71.2	75.5	80.3	86.6	55.3	48.3	58.7	45.0	49.9	59.0
<b>WSARL</b>	✓	✓		✓	✓	<b>50.4</b>	35.1	<b>51.1</b>	<b>74.4</b>	<b>77.1</b>	<b>81.6</b>	<b>86.9</b>	57.8	<b>48.9</b>	58.8	48.7	<b>54.2</b>	<b>60.4</b>

**Attention Learning** S-Net learns spatial attentions of each AU and increases the average F1-frame to 56.2 over B-Net. There are implicit attention mechanisms in deep neural networks (DNN) (Zhao, Chu, and Zhang 2016). The spatial attention learning here explicitly learns spatial attentions and uses them to weight DNN features. By adding the channel-wise attention mechanism explicitly, SC-Net further improves the performance. Note that these spatial attention learning and channel-wise attention learning can achieve better performance when integrated with the multi-scale region learning and the relation learning.

**Multi-Scale Region Learning** Another baseline network, SCH-Net, further incorporates the hierarchical and multi-scale region layer. By processing multi-scale patches with independent filters, SCH-Net increases the result over SC-Net significantly. By removing the hierarchical structure of the hierarchical and multi-scale region layer, SCM-Net further improves the performance. The large margin 2.4 between the result of SCM-Net and that of SC-Net demonstrates that our multi-scale region learning can extract useful features to facilitate the channel-wise and spatial attention learning.

**Relation Learning** Base on SCM-Net, our WSARL further introduces the pixel-level relation learning to refine spatial attentions of each AU. By exploiting the relations between each pair of pixels, WSARL achieves the best average F1-frame result of 60.4. The outstanding performance of WSARL is attributed to the integration of the attention learning, the relation learning, and the multi-scale region learning.

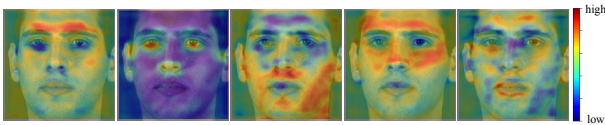


Figure 4: Visualization of several attentive channels of  $f_i^{(c)}$  in Eq. 4 for AU 24. Colors on each channel indicate different values from low to high, as shown in the color bar.

## Qualitative Results

**Channel-Wise Attention Learning** Taking AU 24 of BP4D as an example, several channels of  $f_i^{(c)}$  in Eq. 4 are visualized in Figure 4. To observe the pattern detected by the

corresponding filter of each channel, the visualized results are overlaid on the input image. We can observe that different filters emphasize on different facial attributes. In particular, the first channel emphasizes on the forehead, and the second channel detects distinctive facial regions including the eyes, nose, and ears. The third and the fourth emphasize on lower parts and upper parts of a face respectively, and the fifth detects remaining facial regions including the distinctive mouth. Therefore our channel-wise attention learning can select features generated by the filters which detect the patterns related to AU detection. Note that the selected features are rich, which will be further processed by the spatial attention learning and the pixel-level relation learning.

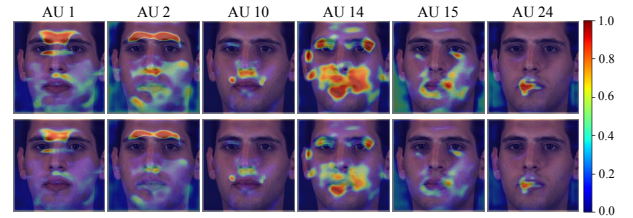


Figure 5: Visualization of  $v_i^{(ous)}$  and  $v_i^{(s)}$  of an example image from BP4D, which are shown in the first row and the second row, respectively. Attention weights are visualized with the colors defined in the color bar.

**Pixel-Level Relation Learning** To investigate the effect of our pixel-level relation learning on spatial attentions, we visualize the initial spatial attention weights  $v_i^{(ous)}$  and refined spatial attention weights  $v_i^{(s)}$  for several AUs of an example image in Figure 5. It can be seen that the refined spatial attentions are smoother with small isolated regions being removed. Taking AU 2 as an example, the noisy attentions in the regions of cheeks, profiles, and mouth are significantly reduced, and the correct attentions in the region of brow are preserved. Moreover, the useless attentions in the background are removed, as shown in the AUs 2, 15, and 24. Thus our pixel-level relation learning is beneficial for capturing more accurate attentions and extracting more relevant local features.

**WSARL** Here we illustrate that our framework WSARL can find the ROIs of AUs and capture the relations among AUs. In particular, we visualize the refined spatial attention

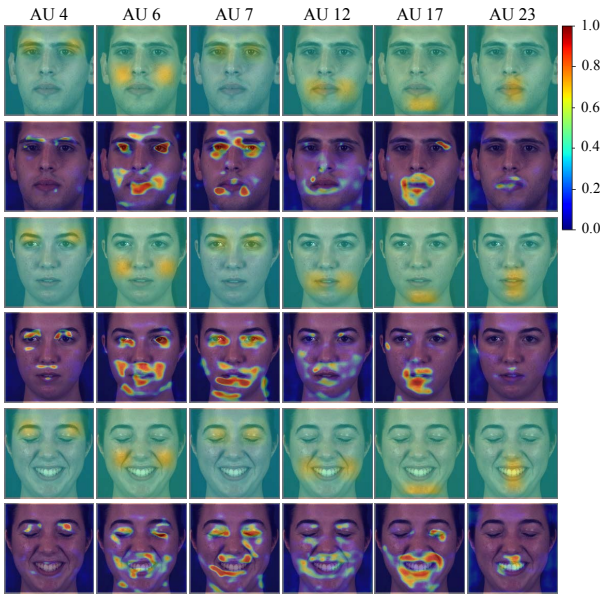


Figure 6: Visualization of the refined spatial attention weights of three BP4D images. Every two rows show the results of the same image, where the first, third, and fifth rows show the results of JAA (Shao et al. 2018), and the second, fourth, and sixth rows show the results of our method WSARL. The first and second images have the same facial expression, and the second and third images are from the same person with different expressions. Attention weights are visualized with the colors defined in the color bar.

weights of WSARL and JAA (Shao et al. 2018) for several AUs of example images in Figure 6. There are two interesting observations from the visualization results as follows:

- The ROI of each AU has an attention distribution which should change across persons and facial expressions. It can be observed that the learned spatial attentions of JAA are very similar for the same AU of different images. In contrast, for WSARL, the first and second images show that the ROIs of the same AU from different persons with the same expression have different attentions. Moreover, the second and third images show that the ROIs of the same AU from the same person with different expressions also have different attentions. Note that our learned spatial attentions in general agree with those of JAA that is based on landmark priors, but with much more details. This demonstrates the effectiveness of our WSARL.
- Using the attentions of JAA as the reference, the highlighted attentions of our WSARL occur in the ROIs of both current AU and other closely related AUs. For example, AUs 6 and 7 have similar attentions, which suggests the close relations between AUs 6 and 7. In addition, AU 6 has attentions in the ROI of AU 23, which indicates the slight relations between AUs 6 and 23. Also, according to the learned attentions, we can see that AU 4 has no relation to AUs 17 and 23. Therefore our pixel-level relation learning captures three types of relations among AUs in-

cluding close relations, slight relations, and no relation. In contrast, the spatial attentions of JAA are not highlighted in correlated regions beyond the predefined ROIs. Thus, it fails to capture the relations among AUs.

Moreover, for those AUs that are not distinct, their ROIs are difficult to be predefined by landmarks. For example, the location relationships between landmarks and AUs 9, 25, and 26 of DISFA benchmark are not defined in the previous works (Li et al. 2017; Sanchez, Tzimiropoulos, and Valstar 2018; Shao et al. 2018). Here we visualize  $\mathbf{v}_i^{(s)}$  of our WSARL for the three AUs in Figure 7, where the images are suffered from glasses occlusion and illumination variations. It can be seen that WSARL is robust to occlusion and illumination variations, and can adaptively learn spatial attentions of different persons with various expressions.

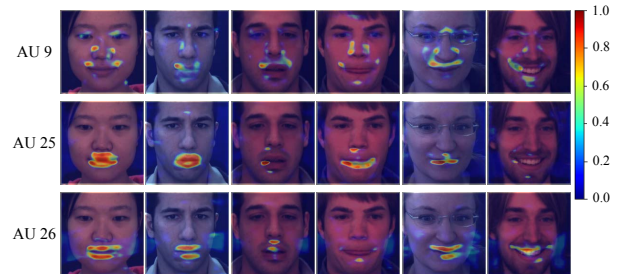


Figure 7: Visualization of  $\mathbf{v}_i^{(s)}$  of our WSARL for AUs 9, 25, and 26 of DISFA benchmark. Attention weights are visualized with the colors defined in the color bar.

## Conclusion

In this paper, we have proposed a novel end-to-end weakly-supervised attention and relation learning framework for AU detection. Both channel-wise attention learning and spatial attention learning are used to select and extract AU related features with only AU labels. Moreover, we have also incorporated the pixel-level relation learning to refine spatial attentions so as to extract more accurate local features. Extensive experiments have demonstrated that our framework outperforms the state-of-the-art methods for AU detection, and can find the ROI of each AU and capture the relations among AUs adaptively. We believe that the idea of weakly-supervised attention and relation learning is also promising for other face analysis tasks such as facial expression recognition and face recognition.

## Acknowledgments

This work was supported by the National Natural Science Foundation of China (No. 61503277 and No. 61472245). It was also partially supported by Data Science & Artificial Intelligence Research Centre@NTU (DSAIR), SINGTEL-NTU Cognitive & Artificial Intelligence Joint Lab (SCALE@NTU), and the joint project of Tencent YouTu and Shanghai Jiao Tong University.

## References

- Chen, L.-C.; Papandreou, G.; Kokkinos, I.; Murphy, K.; and Yuille, A. L. 2017. Deeplab: Semantic image segmentation with deep convolutional nets, atrous convolution, and fully connected crfs. *IEEE Transactions on Pattern Analysis and Machine Intelligence* 40(4):834–848.
- Ekman, P., and Rosenberg, E. L. 1997. *What the face reveals: Basic and applied studies of spontaneous expression using the Facial Action Coding System (FACS)*. Oxford University Press, USA.
- Eleftheriadis, S.; Rudovic, O.; and Pantic, M. 2015. Multi-conditional latent variable model for joint facial action unit detection. In *IEEE International Conference on Computer Vision*, 3792–3800. IEEE.
- Fan, R.-E.; Chang, K.-W.; Hsieh, C.-J.; Wang, X.-R.; and Lin, C.-J. 2008. Liblinear: A library for large linear classification. *Journal of Machine Learning Research* 9(Aug):1871–1874.
- Ioffe, S., and Szegedy, C. 2015. Batch normalization: Accelerating deep network training by reducing internal covariate shift. In *International Conference on Machine Learning*, 448–456.
- Jia, Y.; Shelhamer, E.; Donahue, J.; Karayev, S.; Long, J.; Girshick, R.; Guadarrama, S.; and Darrell, T. 2014. Caffe: Convolutional architecture for fast feature embedding. In *ACM International Conference on Multimedia*, 675–678. ACM.
- Kuen, J.; Wang, Z.; and Wang, G. 2016. Recurrent attentional networks for saliency detection. In *IEEE Conference on Computer Vision and Pattern Recognition*, 3668–3677. IEEE.
- Li, W.; Abtahi, F.; and Zhu, Z. 2017. Action unit detection with region adaptation, multi-labeling learning and optimal temporal fusing. In *IEEE Conference on Computer Vision and Pattern Recognition*, 6766–6775. IEEE.
- Li, W.; Abtahi, F.; Zhu, Z.; and Yin, L. 2017. Eac-net: A region-based deep enhancing and cropping approach for facial action unit detection. In *IEEE International Conference on Automatic Face & Gesture Recognition*, 103–110. IEEE.
- Lin, M.; Chen, Q.; and Yan, S. 2014. Network in network. In *International Conference on Learning Representations*.
- Lucey, P.; Cohn, J. F.; Kanade, T.; Saragih, J.; Ambadar, Z.; and Matthews, I. 2010. The extended cohn-kanade dataset (ck+): A complete dataset for action unit and emotion-specified expression. In *IEEE Conference on Computer Vision and Pattern Recognition Workshops*, 94–101. IEEE.
- Martinez, B.; Valstar, M. F.; Jiang, B.; and Pantic, M. 2017. Automatic analysis of facial actions: A survey. *IEEE Transactions on Affective Computing* PP(99):1–1.
- Mavadati, S. M.; Mahoor, M. H.; Bartlett, K.; Trinh, P.; and Cohn, J. F. 2013. Disfa: A spontaneous facial action intensity database. *IEEE Transactions on Affective Computing* 4(2):151–160.
- Nair, V., and Hinton, G. E. 2010. Rectified linear units improve restricted boltzmann machines. In *International Conference on Machine Learning*, 807–814.
- Newell, A.; Yang, K.; and Deng, J. 2016. Stacked hourglass networks for human pose estimation. In *European Conference on Computer Vision*, 483–499. Springer.
- Sanchez, E.; Tzimiropoulos, G.; and Valstar, M. 2018. Joint action unit localisation and intensity estimation through heatmap regression. In *British Machine Vision Conference*. BMVA Press.
- Shao, Z.; Liu, Z.; Cai, J.; and Ma, L. 2018. Deep adaptive attention for joint facial action unit detection and face alignment. In *European Conference on Computer Vision*. Springer.
- Wu, Y., and Ji, Q. 2016. Constrained joint cascade regression framework for simultaneous facial action unit recognition and facial landmark detection. In *IEEE Conference on Computer Vision and Pattern Recognition*, 3400–3408. IEEE.
- Xiao, T.; Xu, Y.; Yang, K.; Zhang, J.; Peng, Y.; and Zhang, Z. 2015. The application of two-level attention models in deep convolutional neural network for fine-grained image classification. In *IEEE Conference on Computer Vision and Pattern Recognition*, 842–850. IEEE.
- You, Q.; Jin, H.; Wang, Z.; Fang, C.; and Luo, J. 2016. Image captioning with semantic attention. In *IEEE Conference on Computer Vision and Pattern Recognition*, 4651–4659.
- Zhang, X., and Mahoor, M. H. 2016. Task-dependent multi-task multiple kernel learning for facial action unit detection. *Pattern Recognition* 51:187–196.
- Zhang, X.; Yin, L.; Cohn, J. F.; Canavan, S.; Reale, M.; Horowitz, A.; Liu, P.; and Girard, J. M. 2014. Bp4d-spontaneous: a high-resolution spontaneous 3d dynamic facial expression database. *Image and Vision Computing* 32(10):692–706.
- Zhang, Q.; Wu, Y. N.; and Zhu, S.-C. 2018. Interpretable convolutional neural networks. In *IEEE Conference on Computer Vision and Pattern Recognition*. IEEE.
- Zhao, K.; Chu, W.-S.; De la Torre, F.; Cohn, J. F.; and Zhang, H. 2016. Joint patch and multi-label learning for facial action unit and holistic expression recognition. *IEEE Transactions on Image Processing* 25(8):3931–3946.
- Zhao, K.; Chu, W.-S.; and Zhang, H. 2016. Deep region and multi-label learning for facial action unit detection. In *IEEE Conference on Computer Vision and Pattern Recognition*, 3391–3399. IEEE.
- Zheng, S.; Jayasumana, S.; Romera-Paredes, B.; Vineet, V.; Su, Z.; Du, D.; Huang, C.; and Torr, P. H. 2015. Conditional random fields as recurrent neural networks. In *IEEE International Conference on Computer Vision*, 1529–1537. IEEE.
- Zhong, L.; Liu, Q.; Yang, P.; Huang, J.; and Metaxas, D. N. 2015. Learning multiscale active facial patches for expression analysis. *IEEE Transactions on Cybernetics* 45(8):1499–1510.